Proceedings of the 1st Marine Energy Technology Symposium
METS2013
April 10-11, 2013, Washington, D.C.

OCEAN WAVE PREDICTION FROM NOISY SENSOR MEASUREMENTS*

Basel Alnajjab
ECE Dept., Lehigh University
Bethlehem, PA, 18015

Rick S. Blum†
ECE Dept., Lehigh University
Bethlehem, PA, 18015

ABSTRACT

A multitude of sensor types are investigated for the short-term prediction of the exact time waveforms of ocean waves. a vital component of the optimal control of Wave Energy Converter (WEC) devices. Ocean waves are described as a sum of several plane waves of different frequencies and directions of travel while sensor measurements are assumed to be observed under Gaussian noise. A general expression for the Cramer Rao Bound (CRB) of the estimates is derived pertaining to the group of sensors analyzed in the paper. Recommended sensor types and sensor layouts are suggested for single frequency/direction environments after studying the CRB. Illustrative numerical results supporting these recommendations are provided from a comprehensive study.

1 Introduction

With the aim of enhancing the power output of their devices, companies in the wave energy technology field can utilize advanced control systems to assist them in controlling their devices more optimally. Such systems require accurate ocean wave waveform predictions and are estimated to enhance the efficiency of these devices to twice its current value [1], potentially allowing wave energy to overcome its biggest obstacle and moving it closer to becoming the renewable energy of choice. Although the idea of using prediction of future wave waveforms for improved control of WEC devices is not a new idea [2, 3], no papers studying sensor performance under noise for these environments were found in our literature review while very little related work was found [4, 5]. The authors of [6] [7] discussed using sensors for estimating directional wave spectra and not the exact time waveforms.The papers obtained sensor layout with favorable performance for their specific application and while this paper suggests using a different sensor layout, the knowledge provided by the authors of those papers is surely valuable. Further review seemed to suggest that most prior work concentrated on the statistical description of the waves and not the prediction of the actual waveforms, which is what is needed by the targeted application for the work presented. In this paper, we derive and obtain the Cramer Rao Bound (CRB) for the short-term prediction of the exact time waveforms which would be observed at a particular point in the ocean over a particular range of time.The prediction time is determined by the waves' coherence time so although results presented in the paper are for 100s ahead, in real world applications that time can change to be a longer or a shorter time without affecting the findings presented in the paper. We assume the prediction is based on noisy measurements taken from a set of distributed sensors. The CRB is a lower bound on the minimum mean square prediction error that can be achieved by any unbiased estimator, an estimator that produces zero error on average. Thus, a low CRB is desirable as it indicates a smaller error in wave prediction and a better power output from the WEC device. The results will be used to analyze the prediction errors for all the popular fluid flow characterizations that one might want to predict, including all of the quantities listed in Table 1. The sensors employed can also measure any of the quantities listed in Table 1, which includes most of the multi-component array sensors described in [8]. Note that the sensors can measure quantities which are different from the quantity predicted. Further, we will show advantages for choosing sensors which measure something distinctly different from what we seek to predict. In this paper we analyze the CRB for different sensors and predicted quantities in an attempt to describe the best sensor choices and layouts for single frequency/direction ocean environments, which is a first step towards understanding more complicated environments.

For our analysis, we use the well accepted standard wave

*THIS WORK WAS SUPPORTED BY THE NATIONAL SCIENCE FOUNDATION UNDER GRANT CCF-0829958.

†Corresponding Author:rblum@lehigh.edu

equation model from [9] where we assume the ocean is an ideal incompressible fluid with no loss of mechanical energy. We also adopt the common assumptions that the fluid motion is irrotational and that the wave amplitudes are small enough so that linear theory is applicable. Moreover, the monitoring area in the ocean is assumed to be of sufficient depth such that finite depth effects, other than dispersion, are small. Finally, we assume that the waves were created by forcing functions, distant storms for example, that were applied at sufficient distances away resulting in the observation of fully developed ocean waves. Under the assumptions just described, the solutions for the simplified differential equation are plane waves consisting of a sum of sinusoids with different amplitudes, frequencies, directions, wavelengths and phases. Therefore, we assume there are exactly M plane waves each with L frequency components in the part of the ocean being monitored. Then for all two dimensional sensor locations $(x,y)^T$ on the surface, all times t of interest and any of the popular fluid flow characterizations from Table 1 that one might want to predict, the exact time waveform which would be observed at a particular point in the ocean is described by

$$\begin{aligned}&\Phi(x,y,t) = \\ &\sum_{i=1}^{M}\sum_{j=1}^{L} A_{i,j} w_j^a \cos^b(\beta_i)\sin^c(\beta_i)\cos^d(\,|k_j|x\cos(\beta_i)+ \\ &|k_j|y\sin(\beta_i) - tw_j + \phi_{i,j}) \\ &\sin^e(|k_j|x\cos(\beta_i)|k_j| + y\sin(\beta_i) - tw_j + \phi_{i,j})(\frac{1}{g})^f, \end{aligned} \quad (1)$$

where $A_{i,j}$ is the amplitude in meters, ω_j is the frequency in radians per second, β_i is the angular direction in radians measured relative to the x-axis, ϕ_{ij} is the phase in radians and $|k_j|$ is related to ω_j as given in the dispersion relation

$$\omega_j^2 = g|k_j|\tanh(|k_j|h). \quad (2)$$

We are interested in the cases where, for any j, $|k_j|h >> 1$ so we can assume $\tanh(|k_j|h) \approx 1$ in (2) which results in the simplification of the dispersion relationship to

$$\omega_j^2 \approx g|k_j|, \quad (3)$$

and the simplification of (1) to

$$\begin{aligned}&\Phi(x,y,t) = \\ &\sum_{i=1}^{M}\sum_{j=1}^{L} A_{i,j} w_j^a \cos^b(\beta_i)\sin^c(\beta_i)\cos^d\left((\frac{w_j^2}{g})x\cos(\beta_i)+\right. \\ &\left.(\frac{w_j^2}{g})y\sin(\beta_i) - tw_j + \phi_{i,j}\right) \\ &\sin^e(\,(\frac{w_j^2}{g})x\cos(\beta_i) + (\frac{w_j^2}{g})y\sin(\beta_i) - tw_j + \phi_{i,j})(\frac{1}{g})^f. \end{aligned} \quad (4)$$

In (1) and (4) the constants 'a' through 'f' are integer constants used to uniquely determine the ocean flow characterization under consideration. Table 1 shows the values of these constants for popular ocean flow characterizations. From the table, one notices that there exists a group of sensors for which the value of the selection constants 'b' and 'c' are both zero. Measurements by these sensors are wave elevation ($a = 0$), vertical surface velocity ($a = 1$), or vertical surface acceleration ($a = 2$). These sensors' measurements can be thought of as being along the z-axis where the x-y plane represents the ocean surface and the point $z = 0$ describes the flat ocean level in the absence of any waves. Such sensors and their measurements will be categorized as vertical. Measurements from the remaining sensors, where either 'b' is equal to one or 'c' is equal to one, are along the direction of the x-axis ($b = 1$) or the y-axis ($c = 1$) and will be categorized as non-vertical sensors. Non-vertical sensors have corresponding vertical sensor in the sense that they measure the same class of ocean flow characterization (velocity along the x-axis and vertical surface velocity for example). A non-vertical can be obtained from its corresponding measurement by simply multiplying the vertical measurement by either a cosine($b = a$) or a sine ($c = 1$) of the angle describing the wave direction, subtracting a $\pi/2$ phase shift from the argument of the time varying sinusoid for cases where $e = 1$, and diving by the acceleration due to gravity for $f = 1$.

In the following section we formally introduce the Cramer Rao Bound and provide the general equations for calculating the Fisher Information Matrix (FIM) under Gaussian white noise. Section 3 discusses situations that result in a singular FIM. In Section 4, we derive and obtain the FIM under single wave ocean conditions. Section 5 analyzes the performance of multiple sensors based on differences in their FIMs and provides numerical results highlighting the findings. We conclude in the last section and discuss potential further research.

2 Cramer Rao Bounds

To derive the CRB [10] we assume a general sensor measurement described by (4) and we consider a sensor site $r =$

TABLE 1. Integer Constant Values for Selected Predicted Quantities or Sensor Measurements

ine Sensor Measurement	a	b	c	d	e	f
ine Surface Elevation	0	0	0	1	0	0
ine Vertical Surface Velocity	1	0	0	0	1	0
ine Vertical Surface Acceleration	2	0	0	1	0	0
ine Displacement(x-axis)	0	1	0	0	1	0
ine Displacement(y-axis)	0	0	1	0	1	0
ine Velocity (x-axis)	1	1	0	1	0	0
ine Velocity (y-axis)	1	0	1	1	0	0
ine Acceleration (x-axis)	2	1	0	0	1	0
ine Acceleration (y-axis)	2	0	1	0	1	0
ine Surface slope (x-axis)	2	1	0	0	1	1
ine Surface slope (y-axis)	2	0	1	0	1	1
ine						

$1,\ldots,N$ defined by a position vector $(x_r,y_r)^T$ and let the noisy sensor measurements at site r be described by

$$\phi(t_m,x_r,y_r) = \Phi(t_m,x_r,y_r) + v_r(t_m), \quad t_m = T_s,\ldots,KT_s \tag{5}$$

where T_s is a sampling period and $v_r(t_m)$ is Gaussian white noise. Collect the unknown parameters in (4) in the vector

$$\theta = (A_{11},\ldots,A_{ML},\beta_1,\ldots,\beta_M,\omega_1,\ldots,\omega_L,\phi_{11},,\ldots,\phi_{ML})^T, \tag{6}$$

which is an $2ML+M+L$ dimensional vector. For simplicity assume

$$(v_1(T_s),\ldots,v_N(T_s),\ldots,v_1(KT_s),\ldots,v_N(KT_s))^T$$

is a jointly Gaussian vector with zero mean vector and covariance matrix which is diagonal with $(\sigma_1^2,\ldots,\sigma_{NK}^2)$ along the diagonal, then the joint probability density function (pdf) of the observations conditioned on θ, often called the likelihood function,is

$$f_{\underline{\Phi}}(\underline{\Phi};\theta) = \prod_{r=1}^{N}\prod_{k=1}^{K}\frac{1}{\sqrt{2\pi\sigma_{r,k}^2}} \exp\left(-\frac{(\phi(kT_s,x_r,y_r)-\Phi(kT_s,x_r,y_r))^2}{2\sigma_{r,k}^2}\right). \tag{7}$$

Let $\hat{\Phi}(x_p,y_p,t_p)$ be an unbiased estimator of the quantity we are trying to predict $\Phi(x_p,y_p,t_p)$, which is $\Phi(x,y,t)$ from (4) at a particular location (x_p,y_p) and time t_p. Unbiased estimators are those satisfying the equation

$$E_\theta\left\{\hat{\Phi}(x_p,y_p,t_p)\right\} = \Phi(x_p,y_p,t_p). \tag{8}$$

Then [11, 12] the mean-square error (MSE), or variance, of any unbiased estimate must satisfy

$$MSE_{\hat{\Phi}(x_p,y_p,t_p)} \geq qJ(\theta)^{-1}q^T = CRB_{\hat{\Phi}(x_p,y_p,t_p)}, \tag{9}$$

where the quantity on the right hand side of (9) is called the CRB of the estimate $\hat{\Phi}(x_p,y_p,t_p)$. From (9), the CRB is defined in terms of the row vector

$$q = \left(\frac{\partial\Phi(x_p,y_p,t_p)}{\partial\theta_1},\ldots,\frac{\partial\Phi(x_p,y_p,t_p)}{\theta_{2ML+M+L}}\right). \tag{10}$$

and the $(2ML+M+L)\times(2ML+M+L)$ Fisher information matrix (FIM) matrix $\mathbf{J}(\theta)$. As a reminder to the reader, a lower CRB is desired as it indicates a smaller error in prediction and from (9) it can be seen that a lower CRB is equivalent to a larger FIM. The $\ell - n^{th}$ entry of the FIM is calculated as [11, 12]

$$J_{\ell,n}(\theta) = E\left\{\frac{\partial}{\partial\theta_\ell}\ln f_{\underline{\Phi}}(\underline{\Phi};\theta)\frac{\partial}{\partial\theta_n}\ln f_{\underline{\Phi}}(\underline{\Phi};\theta)\right\}. \tag{11}$$

For our case where we consider Gaussian noise, (11) has a general form given by

$$J_{\ell,n}(\theta) = \sum_{r=1}^{N}\sum_{k=1}^{K}\frac{1}{\sigma_{r,k}^2}\left(\frac{\partial}{\partial\theta_\ell}\Phi(x_r,y_r,kT_s)\right)\left(\frac{\partial}{\partial\theta_n}\Phi(x_r,y_r,kT_s)\right) \tag{12}$$

where we see that calculating each entry in the FIM will involve the product of two derivatives where each is derived according to whether $\theta_i, i = 1,2,\ldots,2ML+M+L$ corresponds to amplitude, direction, frequency or phase. As an example, if we consider the simple case where the ocean environment is defined by a single wave ($M = L = 1$), the vector of wave parameters (6) is

$$\theta = (A_{11},\beta_1,\omega_1,\phi_{11},)^T \tag{13}$$

and the FIM is a 4×4 matrix that is calculated according to (12) as

$$\mathbf{J}(\theta) = \begin{bmatrix} J_{1,1} & J_{1,2} & J_{1,3} & J_{1,4} \\ J_{1,2} & J_{2,2} & J_{2,3} & J_{2,4} \\ J_{1,3} & J_{2,3} & J_{3,3} & J_{3,4} \\ J_{1,4} & J_{2,4} & J_{3,4} & J_{4,4} \end{bmatrix}. \quad (14)$$

We have obtained expressions for the derivatives of any ocean fluid flow characterization described by (4). The expressions are

$$\frac{\partial}{\partial A_{i,j}}\Phi(x_r, y_r, t) = w_j^{a_r} \cos(\beta_i)^{b_r} \sin(\beta_i)^{c_r} \alpha^{d_r} \gamma^{e_r} (\frac{1}{g})^{f_r}, \quad (15)$$

$$\begin{aligned} &\frac{\partial}{\partial \beta_i}\Phi(x_r, y_r, t) = \sum_{j=1}^{L} \\ &(\frac{1}{g})^{f_r+1} A_{i,j} w_j^{a_r} \cos(\beta_i)^{b_r-1} \sin(\beta_i)^{c_r-1} \alpha^{d_r-1} \gamma^{e_r-1} (-b_r g \alpha\, \gamma \\ &+ b_r g \alpha \gamma \cos(\beta_i)^2 + c_r \cos(\beta_i)^2 g \alpha \gamma + d_r w_j^2 x \cos(\beta_i) \\ &- d_r w_j^2 x \cos(\beta_i)^3 - d_r w_j^2 \cos(\beta_i) x \alpha^2 + d_r w_j^2 \cos(\beta_i)^3 x \alpha^2 \\ &- d_r w_j^2 y \cos(\beta_i)^2 \sin(\beta_i) + d_r w_j^2 y \cos(\beta_i)^2 \sin(\beta_i) y \alpha^2 \\ &- e_r \alpha^2 w_j^2 x \cos(\beta_i) + e_r \alpha^2 w_j^2 x \cos(\beta_i)^3 + e_r \alpha^2 w_j^2 \cos(\beta_i)^2 \sin(\beta_i) y \Big), \end{aligned} \quad (16)$$

$$\begin{aligned} &\frac{\partial}{\partial w_j}\Phi(x_r, y_r, t) = \sum_{i=1}^{M} (\frac{1}{g})^{f_r+1} \\ &A_{i,j} w_j^{a_r-1} \Big(\cos(\beta_i)^{b_r} \sin(\beta_i)^{c_r} \alpha^{d_r-1}\, \gamma^{e_r-1} \\ &(a_r g \alpha\, \gamma - 2 d_r w_j^2 x \cos(\beta_i) + 2 d_r w_j^2 x \cos(\beta_i) \alpha^2 - 2 d_r w_j^2 y \sin(\beta_i) \\ &+ 2 d_r w_j^2 y \sin(\beta_i) \alpha^2 + d_r w_j g t - d_r w_j g t \alpha^2 + 2 e_r \alpha)^2 w_j^2 \cos(\beta_i) x \\ &+ 2 e_r \alpha^2 w_j^2 y \sin(\beta_i)\ - e_r \alpha^2 w_j g t \Big) \Big), \end{aligned} \quad (17)$$

and

$$\begin{aligned} &\frac{\partial}{\partial \phi_{i,j}}\Phi(x_r, y_r, t) = \\ &(\frac{1}{g})^{f_r} A_{i,j} w_j^{a_r} \cos(\beta_i)^{b_r} \sin(\beta_i)^{c_r} \alpha^{d_r-1} \gamma^{e_r-1} (-d_r \gamma^2 + e_r \alpha^2), \end{aligned} \quad (18)$$

where we define

$$\alpha = \cos\left(\frac{w_j^2 x_r \cos(\beta_i) + w_j^2 y_r \sin(\beta_i) - t w_j g + \phi_{i,j} g}{g} \right) \quad (19)$$

and

$$\gamma = \sin\left(\frac{w_j^2 x_r \cos(\beta_i) + w_j^2 y_r \sin(\beta_i) - t w_j g + \phi_{i,j} g}{g} \right). \quad (20)$$

3 Singularities in the Fisher Information Matrix

A singular FIM indicates that an estimator would produce large errors. A study of the FIM for our case reveals that there are several conditions that will result in having a FIM that is singular. The most obvious case occurs when a non-vertical sensor is used in an ocean condition described by a direction that is perpendicular to the direction that it measures. For example, this will occur when a sensor that measures displacement along the x-axis is used in an ocean condition with waves traveling along the y-axis as all its measurement will be equal to zero. This exposes a drawback for using non-vertical sensors since their measurements are scaled by a sine or a cosine which are at most equal to 1 and decrease monotonically to zero (where the FIM is singular and the CRB diverges) as one varies wave direction to become closer the direction causing the singularity.

The FIM can also become singular when an insufficient number of measurements is collected. Measurements can be thought of as either temporal measurements that are obtained from a single sensor at various time points or spatial measurements that are obtained from various sensor locations at a single time point. The total number of measurements collected is insufficient if it is less than the number of unknown variables in (6). Also, if the measurements do not allow for the separation of the spatially-dependent terms and the initial phase inside the argument of the sinusoidal term in (4) then the term having the directional dependence is inseprable from the initial phase and the FIM will be singular as it is unable to solve for the wave direction.To explain this, we will consider an ocean environment described by a single wave. The extension of the concept to multiple waves is straightforward. If we consider the attempt to estimate the wave direction and initial phase of a single wave based on temporal measurements from a single sensor, then all space-dependent terms that are inside the argument of the sinusoidal term for any wave characterization from Table 1 are constant and so is the initial phase, making them add up to a single constant value. Then, any wave direction and initial phase that add up to the value of that constant are a possible solution and no information is available about their true values. This forces the FIM to be singular. To overcome this problem, more spatial measurements are needed to provide information allowing for the separation of the two terms. This idea extends to ocean environments described by multiple waves where more spatial measurements (number of sensors) are needed to be able to distinguish between the different spatial terms and the initial phases.

4 The Fisher Information Matrix Under a Single Wave Environment

To obtain a first order understanding of the sensors' behavior, we will use the expressions given in (15)-(18) under the assumption that the ocean environments faced can be described by a single wave ($M = L = 1$). Further we assume that uncertainties in sensor measurements can be modeled as noise and that the noise at each sensor can be considered to be independent and identically distributed ($\sigma_1 = \sigma_2 = \cdots = \sigma_{NK}$). We also restrict the area considered for placing the sensors to a finite area around the origin of our grid to disallow placing sensors at infinitly distant locations where our model for the ocean environment becomes invalid.

4.1 Single Wave Ocean Environment Using a Single Type of Vertical Sensor Measurements

For this section, we consider estimating the wave parameters of an ocean environment (4) described by a single wave ($M = L = 1$) through using multiple sensors of a single type. This section relates to cases when the type used is selected to be one of the vertical sensors in Table 1. In other words the sensors either measure wave elevation, vertical surface velocity, or vertical surface acceleration. To change the sensor type in the equations below, we need only change the the value of the selection constant 'a' according in Table 1. The derivatives (15)-(18) needed for calculating the FIM entries are given as

$$\frac{\partial}{\partial A_{1,1}}\Phi(x,y,t) = w_1{}^a \cos\left((\frac{w_1^2}{g})x\cos(\beta_1)+(\frac{w_1^2}{g})y\sin(\beta_1)-tw_1+\phi_{1,1}\right), \quad (21)$$

$$\frac{\partial}{\partial \beta_1}\Phi(x,y,t) = -A_{1,1}w_1{}^a \sin\left((\frac{w_1^2}{g})x\cos(\beta_1)+(\frac{w_1^2}{g})y\sin(\beta_1)-tw_1+\phi_{1,1}\right) \left((\frac{w_1^2}{g})y\cos(\beta_1)-(\frac{w_1^2}{g})x\sin(\beta_1)\right), \quad (22)$$

$$\frac{\partial}{\partial w_1}\Phi(x,y,t) = -A_{1,1}w_1{}^a \sin\left((\frac{w_1^2}{g})x\cos(\beta_1)+(\frac{w_1^2}{g})y\sin(\beta_1) -tw_1+\phi_{1,1}\right)\left((\frac{2w_1}{g})x\cos(\beta_1)+(\frac{2w_1}{g})y\sin(\beta_1)-t\right) + aA_{1,1}w_1{}^{a-1}\cos\left((\frac{w_1^2}{g})x\cos(\beta_1)+(\frac{w_1^2}{g})y\sin(\beta_1)-tw_1+\phi_{1,1}\right), \quad (23)$$

and

$$\frac{\partial}{\partial \phi_{1,1}}\Phi(x,y,t) = -A_{1,1}w_1{}^a \sin\left((\frac{w_1^2}{g})x\cos(\beta_1)+(\frac{w_1^2}{g})y\sin(\beta_1)-tw_1+\phi_{1,1}\right). \quad (24)$$

Note that we need not include a subscript for the selection constant 'a' since we are considering sensor networks of a single sensor type ($a_r = a$ for all r). From (12) we can see the calculation of each entry in the FIM involves a product of two of the derivatives just given summed over time and sensor location. Assuming that the sampling period T_s is sufficiently small, and that the number of time samples, K, is sufficiently large, we will now attempt to approximate the values of these sums.

First, we start with the diagonal entries of the FIM, starting with the $J_{1,1}$ term

$$\begin{aligned} J_{1,1}(\theta) &= \frac{1}{\sigma^2}\sum_{r=1}^{N}\sum_{k=1}^{K}\left(\frac{\partial}{\partial A_{1,1}}\Phi(x_r,y_r,kT_s)\right)\left(\frac{\partial}{\partial A_{1,1}}\Phi(x_r,y_r,kT_s)\right) \\ &= \frac{{w_1}^{2a}}{\sigma^2}\sum_{r=1}^{N}\sum_{k=1}^{K}\cos^2(\psi - w_1 kT_s) \\ &= \frac{{w_1}^{2a}}{\sigma^2}\sum_{r=1}^{N}\sum_{k=1}^{K}\frac{1}{2}(1+\cos(2\psi-2w_1kT_s)) \\ &\approx \frac{{w_1}^{2a}}{\sigma^2}\sum_{r=1}^{N}\sum_{k=1}^{K}\frac{1}{2} = \frac{NKw_1{}^{2a}}{2\sigma^2}, \end{aligned} \quad (25)$$

where $\psi = (\frac{w_1^2}{g})x_r\cos(\beta_1)+(\frac{w_1^2}{g})y_r\sin(\beta_1)+\phi_{1,1}$ represents the time-independent part of the argument of the cosine function. Notice that the sinusoidal term in the sum can be dropped since $\sum_{k=1}^{K}\cos(2\psi-2w_1kT_s) \le 2$ for any K and its contribution will be insignificant for a large K when added to the contribution from summing 1 for K times. It can be seen that sensor location has little effect on the final value of this term. Now, we consider the more interesting $J_{2,2}$ entry

$$\begin{aligned} J_{2,2}(\theta) &= \frac{1}{\sigma^2}\sum_{r=1}^{N}\sum_{k=1}^{K}\left(\frac{\partial}{\partial \beta_1}\Phi(x_r,y_r,kT_s)\right)\left(\frac{\partial}{\partial \beta_1}\Phi(x_r,y_r,kT_s)\right) \\ &= \frac{A_{1,1}^2 w_1^{4+2a}}{g^2\sigma^2}\sum_{r=1}^{N}((x_r,y_r)\cdot U_{\beta_1})^2\sum_{k=1}^{K}\frac{1}{2}(1-\cos(2\psi-2w_1kT_s)) \\ &\approx \frac{KA_{1,1}^2 w_1^{4+2a}}{2g^2\sigma^2}\sum_{r=1}^{N}((x_r,y_r)\cdot U_{\beta_1})^2, \end{aligned} \quad (26)$$

where $U_{\beta_1} = (-\sin(\beta_1),\cos(\beta_1))$ is the unit vector perpendicular to the wave direction β_1. We can see, that for a known wave

direction β_1, sensors placed as far away as possible in a direction perpendicular to the wave's direction yield the largest possible value for the sum over space and thus maximize the total value of this term. Sensors placed parallel to the wave direction will minimize its value. Let us now consider the $J_{3,3}$ entry of the FIM, given by

$$\begin{aligned} J_{3,3}(\theta) &= \frac{1}{\sigma^2}\sum_{r=1}^{N}\sum_{k=1}^{K}\left(\frac{\partial}{\partial w_1}\Phi(x_r,y_r,kT_s)\right)\left(\frac{\partial}{\partial w_1}\Phi(x_r,y_r,kT_s)\right) \\ &= \frac{1}{\sigma^2}\sum_{r=1}^{N}\sum_{k=1}^{K}\Bigg(-A_{1,1}{w_1}^{a}\sin(\psi-kT_s w_1) \\ &\left(\frac{2w_1}{g}((x_r,y_r)\cdot V_{\beta_1})-kT_s\right)+aA_{1,1}{w_1}^{a-1}\cos(\psi-kT_s w_1)\Bigg)^2, \end{aligned} \tag{27}$$

where $V_{\beta_1}=(\cos(\beta_1),\sin(\beta_1))$ is the unit vector parallel to the wave direction. For sufficiently large K, this term is also maximized if the sensors are placed as far away as possible and perpendicular to the wave direction β_1. This term is hard to approximate with a simpler expression due to the complicated derivative with respect to w and we thus provide no approximation for its value but we note that it grows with K. Looking at the expression for the $J_{4,4}$ entry in the FIM

$$\begin{aligned} J_{4,4}(\theta) &= \frac{1}{\sigma^2}\sum_{r=1}^{N}\sum_{k=1}^{K}\left(\frac{\partial}{\partial \phi_{1,1}}\Phi(x_r,y_r,kT_s)\right)\left(\frac{\partial}{\partial \phi_{1,1}}\Phi(x_r,y_r,kT_s)\right) \\ &= \frac{A_{1,1}^2{w_1}^{2a}}{\sigma^2}\sum_{r=1}^{N}\sum_{k=1}^{K}\sin^2(\psi-w_1kT_s) \\ &= \frac{A_{1,1}^2{w_1}^{2a}}{\sigma^2}\sum_{r=1}^{N}\sum_{k=1}^{K}\frac{1}{2}(1-\cos(2\psi-2w_1kT_s) \\ &\approx \frac{A_{1,1}^2{w_1}^{2a}}{\sigma^2}\sum_{r=1}^{N}\sum_{k=1}^{K}\frac{1}{2}=\frac{NKA_{1,1}^2{w_1}^{2a}}{2\sigma^2}, \end{aligned} \tag{28}$$

where, similar to the $J_{1,1}$ entry, sensor location has little effect on the value of the term.

Now we consider the off-diagonal entries. The $J_{1,2}$ entry of the FIM is given by

$$\begin{aligned} J_{1,2}(\theta) &= \frac{1}{\sigma^2}\sum_{r=1}^{N}\sum_{k=1}^{K}\left(\frac{\partial}{\partial A_{1,1}}\Phi(x_r,y_r,kT_s)\right)\left(\frac{\partial}{\partial \beta_1}\Phi(x_r,y_r,kT_s)\right) \\ &= \frac{-A_{1,1}w_1^{2+2a}}{g\sigma^2}\sum_{r=1}^{N}((x_r,y_r)\cdot U_{\beta_1})\sum_{k=1}^{K}\cos(\psi-w_1kT_s)\sin(\psi-w_1kT_s) \\ &\le \frac{A_{1,1}w_1^{2+2a}}{g\sigma^2}\sum_{r=1}^{N}((x_r,y_r)\cdot U_{\beta_1}), \end{aligned} \tag{29}$$

where we use the fact that the sum of a product of two sinusoidal functions of different frequencies is bounded and does not grow with K. The $J_{1,3}$ entry in the FIM is given by

$$\begin{aligned} J_{1,3}(\theta) &= \frac{1}{\sigma^2}\sum_{r=1}^{N}\sum_{k=1}^{K}\left(\frac{\partial}{\partial A_{1,1}}\Phi(x_r,y_r,kT_s)\right)\left(\frac{\partial}{\partial w_1}\Phi(x_r,y_r,kT_s)\right) \\ &= \frac{-1}{\sigma^2}\sum_{r=1}^{N}\sum_{k=1}^{K}\Bigg(A_{1,1}{w_1}^{a}\sin(\psi-kT_s w_1)\left(\frac{2w_1}{g}((x_r,y_r)\cdot V_{\beta_1})-kT_s\right) \\ &+aA_{1,1}{w_1}^{a-1}\cos(\psi-kT_s w_1)\Bigg)\left({w_1}^{a}\cos(\psi-kT_s w_1)\right), \end{aligned} \tag{30}$$

where, again, the derivative with respect to w prevents us from obtaining a simple approximation for the term. The $J_{1,4}$ entry of the FIM is given by

$$\begin{aligned} J_{1,4}(\theta) &= \frac{1}{\sigma^2}\sum_{r=1}^{N}\sum_{k=1}^{K}\left(\frac{\partial}{\partial A_{1,1}}\Phi(x_r,y_r,kT_s)\right)\left(\frac{\partial}{\partial \phi_{1,1}}\Phi(x_r,y_r,kT_s)\right) \\ &= -\frac{A_{1,1}w_1^{2a}}{\sigma^2}\sum_{r=1}^{N}\sum_{k=1}^{K}\cos(\psi-w_1kT_s)\sin(\psi-w_1kT_s) \\ &\le \frac{A_{1,1}w_1^{2a}}{\sigma^2}\sum_{r=1}^{N}1=\frac{NA_{1,1}w_1^{2a}}{\sigma^2}, \end{aligned} \tag{31}$$

where we can see that the sum over the K time samples is of a product of two sinusoidal functions which does not grow with K. The $J_{2,3}$ entry of the FIM, is given by

$$\begin{aligned} J_{2,3}(\theta) &= \frac{1}{\sigma^2}\sum_{r=1}^{N}\sum_{k=1}^{K}\left(\frac{\partial}{\partial w_1}\Phi(x_r,y_r,kT_s)\right)\left(\frac{\partial}{\partial \beta_1}\Phi(x_r,y_r,kT_s)\right) \\ &\approx \frac{1}{\sigma^2}\sum_{r=1}^{N}\sum_{k=1}^{K}A_{1,1}^2w_1^{2a}\sin^2(\psi-w_1kT_s)\left(\frac{2w_1}{g}((x_r,y_r)\cdot V_{\beta_1})-kT_s\right) \\ &\left(\frac{w_1^2}{g}((x_r,y_r)\cdot U_{\beta_1})\right), \end{aligned} \tag{32}$$

where the approximation is validated by arguing that the contribution from terms that do not grow with K is negligible as we assume that K is reasonably large. Intermediate steps were elim-

inated for brevity.The $J_{2,4}$ entry of the FIM, is given by

$$\begin{aligned} J_{2,4}(\theta) &= \frac{1}{\sigma^2}\sum_{r=1}^{N}\sum_{k=1}^{K}\left(\frac{\partial}{\partial\beta_1}\Phi(x_r,y_r,kT_s)\right)\left(\frac{\partial}{\partial\phi_{1,1}}\Phi(x_r,y_r,kT_s)\right) \\ &= \frac{A_{1,1}^2 w_1^{2+2a}}{g\sigma^2}\sum_{r=1}^{N}((x_r,y_r)\cdot U_{\beta_1})\sum_{k=1}^{K}\sin^2(\psi - w_1 kT_s) \\ &\approx \frac{A_{1,1}^2 w_1^{2+2a}}{g\sigma^2}\sum_{r=1}^{N}((x_r,y_r)\cdot U_{\beta_1})\sum_{k=1}^{K}\frac{1}{2} \\ &= \frac{KA_{1,1}^2 w_1^{2+2a}}{2g\sigma^2}\sum_{r=1}^{N}((x_r,y_r)\cdot U_{\beta_1}). \end{aligned} \tag{33}$$

Finally, the last term to consider in the FIM is the $J_{3,4}$ term

$$\begin{aligned} J_{3,4}(\theta) &= \frac{1}{\sigma^2}\sum_{r=1}^{N}\sum_{k=1}^{K}\left(\frac{\partial}{\partial w_1}\Phi(x_r,y_r,kT_s)\right)\left(\frac{\partial}{\partial\phi_1}\Phi(x_r,y_r,kT_s)\right) \\ &= \left(-A_{1,1}{w_1}^a\sin(\psi - kT_s w_1)\left(\frac{2w_1}{g}(x_r,y_r)\cdot V_{\beta_1} - kT_s\right) + \right. \\ &\left. aA_{1,1}{w_1}^{a-1}\cos(\psi - kT_s w_1)\right)\left(-A_{1,1}{w_1}^a\sin(\psi - kT_s w_1)\right) \\ &\approx \frac{A_{1,1}^2 {w_1}^{2a}}{\sigma^2}\sum_{r=1}^{N}\sum_{k=1}^{K}\sin^2(\psi - w_1 kT_s)\left(\frac{2w_1}{g}((x_r,y_r)\cdot V_{\beta_1} - kT_s\right), \end{aligned} \tag{34}$$

where we again drop terms that do not grow with K.

From the analysis just provided, we can see that the $J_{1,2}$ and $J_{1,4}$ terms do not grow with the number of time samples K, unlike all the other terms in the FIM. This will result in these two entries having negligible values when considering the FIM as a whole, allowing us to approximate them as zeros.

4.2 Single Wave Ocean Environment Using a Single Type of Non-Vertical Sensor Measurement

A non-vertical sensor provides measurements along a single direction (the x-axis for example) in the two dimensional plane describing the ocean surface which is assumed to be flat in the absence of waves. A sensor providing measurements along a direction that is perpendicular to the first direction (the y-axis) allows for a complete description of the measurements pertaining to the x-y plane. Non-vertical sensor measurements can be obtained from their corresponding vertical measurements through multiplying the vertical measurement by a $\cos(\beta_1)$ when $b = 1$ or a $\sin(\beta_1)$ when $c = 1$ and subtracting $\pi/2$ from the initial phase when $e = 1$. This means that all the FIM entries that do not depend on the derivative with respect to β_1 are the same as the ones derived for the vertical sensors measurements except that they are multiplied by either a $\cos^2(\beta_1)$ when $b = 1$ or $\sin^2(\beta_1)$ when $c = 1$ while redefining ψ as $\psi = (\frac{w_1^2}{g})x_r\cos(\beta_1) + (\frac{w_1^2}{g})y_r\sin(\beta_1) + \phi_{1,1} - e\frac{\pi}{2}$. Terms involving the derivative with respect to β_1 will have an added term which results from the product rule for differentiation. The derivation of those terms is eliminated from this paper for brevity and to avoid redundancy. Under our assumption of reasonably large K, we have noticed that the extra terms resulting from the product rule have a small effect on the behavior of the FIM and that the effect of multiplying the terms by the $\cos^2(\beta_1)$ when $b = 1$ or $\sin^2(\beta_1)$ when $c = 1$ dictates the total affect on the FIM. The only exception is the $J_{1,2}$ which now grows with K and can no longer be approximated as zero.

This completes deriving a general form for a FIM based on measurements from networks consisting of the same type of sensors where the measurements can be described by (4) and Table 1. Fisher Information matrices relating to heterogeneous networks (networks consisting of more than a single type of sensors) can be easily obtained by dividing the heterogeneous network into multiple homogeneous networks (networks consisting of a single type of sensors). For each homogeneous network, the FIM can be calculated using the equations just derived and then the FIM for the overall network is simply the sum of all the individual FIMs from the homogeneous networks.

5 Performance Based on the FIM and Numerical Results

System designers aim to extract the best performance possible from their sensor networks. The variables controlled by the designers are the positions of the sensors (x_r, y_r) and the type of sensor used $(a_r, b_r, c_r, d_r, e_r, f_r)$ at each position. For obvious reasons, it is impractical to change the type or the position of a sensor after it is deployed which deems it impossible to employ the optimal choice of sensor positions and sensor choice if the optimal decision changes with the changing ocean conditions. As an example, the optimal sensor position for a certain wave direction will change as the direction of the wave changes and since we cannot move sensors after deploying them, having our network operate in a suboptimal setup is inevitable as the ocean environment changes. The sensor choice problem can be easily solved. As mentioned previously, non-vertical sensor measurements relate to their corresponding vertical measurements by a scale factor of either a $\cos(\beta_1)$ or a $\sin(\beta_1)$ and by subtracting $\pi/2$ from the argument of the time varying cosine in equation (4). From the previous section, one can see that the initial phase of the wave has little or no effect on the terms of the FIM. However, scaling every term in the FIM by the square of a sinusoidal function has a great effect on the CRB. To show this mathematically we consider equation (9), the equation for calculating the CRB, where if we let $J(\theta)$ represent the FIM for a vertical sensor, then the FIM for a similar non-vertical sensor

(vertical velocity and velocity in the x direction for example), under the assumption of reasonably large K, can be considered to be $J^*(\theta) \approx \cos^2(\beta_1)J(\theta)$ and the CRB is now approximately equal to

$$CRB^*_{\hat{\Phi}(x_p,y_p,t_p)} \approx q\Big(\cos^2(\beta_1)J(\theta)\Big)^{-1}q^T = \frac{CRB_{\hat{\Phi}(x_p,y_p,t_p)}}{\cos^2(\beta_1)}, \tag{35}$$

where $CRB^*_{\hat{\Phi}(x_p,y_p,t_p)}$ is the CRB for a non-vertical sensor and $CRB_{\hat{\Phi}(x_p,y_p,t_p)}$ is that for a vertical sensor. (35) shows that the CRB for vertical sensors will be smaller, for most cases, than the CRB for its corresponding non-vertical sensors which indicates that the optimal sensor choice will always be one of the three vertical sensors. We note that there exists a small number of special cases where the CRB of a non-vertical sensor can be slightly smaller than that for a vertical sensor. These special cases occur when the wave direction is very close to the value making the sinusoidal function equal to 1 and the phases are such that the CRBs of the different sensors are out of phase. Designing for these special cases entails incurring a large loss in performance if the wave direction changes. Figure 1 shows the change in the CRB obtained from using non-vertical sensors as the wave direction changes. It also shows that vertical sensors show no change in their performance under the different wave directions considered, which reinforces the analysis just provided. The ocean environment in Figure 1 assumed eight sensors, $A_{1,1} = 2m$, $w_1 = 1.6rad/s$, and $\phi_{1,1} = 1rads$ while varying β_1 from 0.3rads to 1.3rads. Sensors were placed evenly spaced on the perimeter of a circle of radius equal to 300m. Time samples were collected for 8 seconds with a sampling frequency of 100Hz. The CRB is calculated for predictions at the origin 100s ahead.

Limiting our attention to the three vertical sensors, the sensors' measurements differ by their value for the selection constant 'a' as given in Table 1. We observed that the effect from the extra terms resulting from the product rule of differentiation has little effect on the task of comparing the sensors types for cases of large K. So if we let $J(\theta)$ be the FIM for a wave elevation sensor ($a = 0$) and let $J^*(\theta) \approx w^{2a}J(\theta)$ be the FIM for using vertical surface velocity sensors ($a = 1$) or vertical surface acceleration sensors ($a = 2$), then the CRBs for the different sensor types can be compared as follows

$$CRB^*_{\hat{\Phi}(x_p,y_p,t_p)} \approx q\Big(w^{2a}J(\theta)\Big)^{-1}q^T = \frac{CRB_{\hat{\Phi}(x_p,y_p,t_p)}}{w^{2a}}, \tag{36}$$

where $CRB_{\hat{\Phi}(x_p,y_p,t_p)}$ is the CRB for elevation sensors and $CRB^*_{\hat{\Phi}(x_p,y_p,t_p)}$ is that for the vertical velocity and vertical acceleration sensors. Radial frequency values for cases of interest vary between $0.25 - 2.0rad/s$. Therefore, according to (36), the optimal sensor choice depends on whether the radial frequency is greater or less than 1. For cases where $w < 1$, the optimal sensor is that having the smallest value for 'a' , which is the wave elevation sensor. For cases where $w > 1$, the optimal sensor is that having the largest value for 'a' , which is the vertical surface acceleration sensor. Figures 2 and 3 illustrate the difference in performance between the two sensors. In both figures, eight sensors are distributed evenly on the perimeter of a circle with a 300m radius and the prediction is made 100s ahead after collecting data for eight seconds at a sampling rate of 100Hz. For Figure 2 the wave parameters were equal to $A_{1,1} = 2m$, $w_1 = 0.6rad/s$, $\beta_1 = \pi/3rads$, and $\phi_{1,1} = 1rads$. For Figure 3 the wave parameters were equal to $A_{1,1} = 2m$, $w_1 = 1.6rad/s$, $\beta_1 = \pi/3rads$, and $\phi_{1,1} = 1rads$. These plots show the CRB of elevation versus the Signal to Noise Ratio (SNR) which is defined as $SNR = 10log_{10}(\frac{{A_{1,1}}^2}{2\sigma^2})$. The figures compare a single pair of parameter values as we have not been able to find any parameter values that would result in an anomaly.

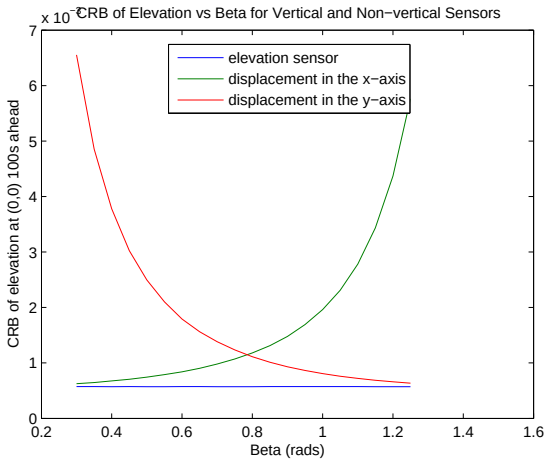

FIGURE 1. Change in the CRB of elevation under varying wave direction for a vertical sensor and its corresponding non-vertical sensors

The problem of optimal sensor placement is complicated for varying ocean wave conditions and predictions at multiple times and positions. Some of the optimization criteria for similar cases attempt to maximize the determinant of the FIM [13] while others focus on the Trace of the inverse of the FIM [14]. Both these criteria favor larger diagonal FIM entries. This agrees with the intuition that the larger the diagonal entries of the FIM, the smaller the variances in the individual unknown parameters in (6). In the previous section, we noted that the $J_{2,2}$ and $J_{3,3}$ terms in the FIM, both diagonal entries, are maximized when the sensors are placed as far as possible along the perpendicular to the direction of travel of the wave. Numerical results showed enhanced performance for layouts where the sensors were placed

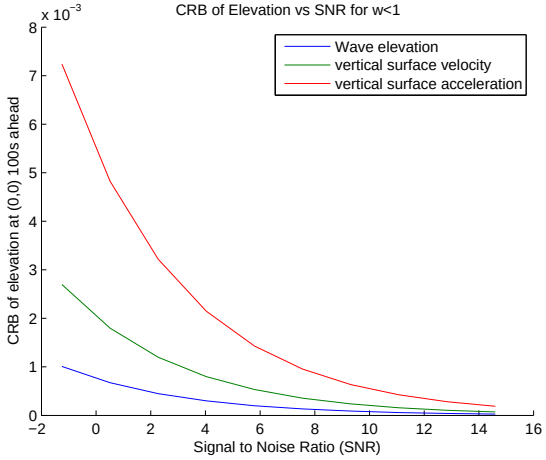

FIGURE 2. CRB of elevation for $w < 1$

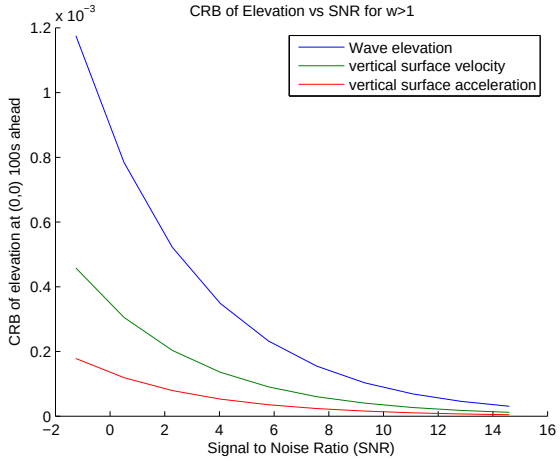

FIGURE 3. CRB of elevation for $w > 1$

perpendicular to the wave direction such that the $J_{2,2}$ and $J_{3,3}$ terms in the FIM are maximized. Therefore, for a given wave direction, it is recommended that the sensors are placed perpendicular to that direction and as far away as possible from each other. For equally likely wave directions, we recommend placing the sensors with equal spacing between them on the arc of two opposing sectors joined at their tip, where the center angle of each sector is equal to the range of possible directions. For example, if eight sensors are used in conditions where waves are equally likely to come from any direction $(0-\pi rads)$, then the sensors should be placed with $\pi/4$ separation on the perimeter of a circle having the maximum allowable radius. Figure 4 demonstrates the recommended layout strategy for the case where eight sensors are used in an environment where the wave direction is equally likely to take any value in a $\pi/4$ rads interval. Under

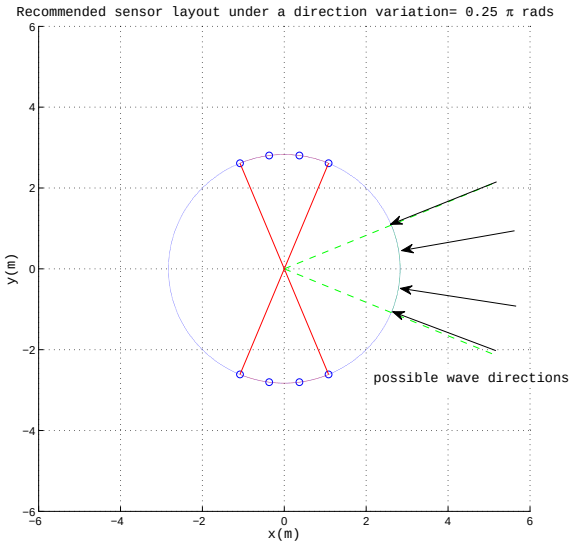

FIGURE 4. Recommended layout strategy under possible wave direction variation of pi/4 . Prediction is made at the origin

this adopted layout, it was found that some off-diagonal terms will have negligible or decreased values which seemed to further enhance the sensors' estimation capability.A good example explaining this observation is the $J_{2,4}$ term

$$J_{2,4}(\theta) \approx \frac{KA_{1,1}^2 w_1^{2+2a}}{2g\sigma^2} \sum_{r=1}^{N} (y_r \cos(\beta_1) - x_r \sin(\beta_1)), \qquad (37)$$

where the sum over space can be thought of as two individual sums; one over the y-coordinates of the sensor positions and the other over the x-coordinates of the sensors positions. Under a 'diagonal maximizing' layout each of these sums will go to zero

$$J_{2,4}(\theta) \approx \frac{KA_{1,1}^2 w_1^{2+2a}}{2g\sigma^2} \left(\cos(\beta_1) \sum_{r=1}^{N} y_r - \sin(\beta_1) \sum_{r=1}^{N} x_r \right) = 0. \qquad (38)$$

Figure 5 compares the performance of two sensors networks that use the same type of sensor under the same wave environment where the waves are equally likely from all directions with the only difference being that the sensors are placed according to the 'diagonal maximizing' layout for one network while they are placed randomly in the other network. Sensors were placed on the perimeter of a circle with radius equal to 300 meters. In Figure 5, the parameter settings are $A_{1,1} = 0.5m$, $w_1 = 1rad/s$, $\beta_1 = 1.79rads$ and $\phi_{1,1} = 2.87rads$. 8 sensors were used and they were always placed on the perimeter of a circle of radius

300m. The prediction point is taken to be the origin and the prediction is made for 100s ahead. Results for the random layout are averaged over a hundred random layout choices. Having eight sensors greatly decreases the probability of having very bad performance for a single wave environment and should ensure that the average performance under the random layout is meaningful and is not distorted due to outliers.

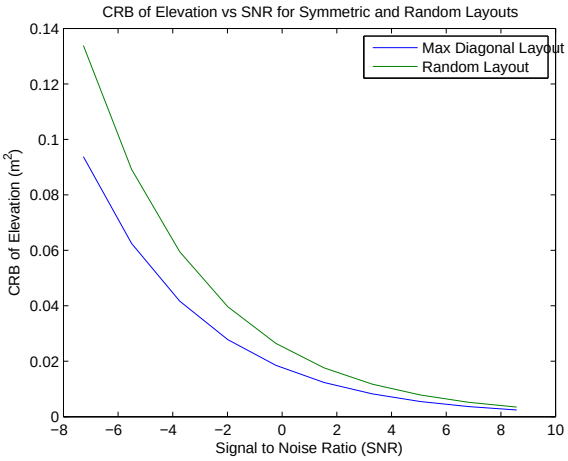

FIGURE 5. CRB of elevation under perpendicular and random layouts

6 Conclusion and Future Work

In conclusion, this paper describes the CRB and provides the necessary equations to calculate it under the assumption the ocean environments can be described as a sum of multiple plane waves. We deduced network design recommendations in terms of sensor choice and sensor layout based on an analysis of the Fisher Information Matrices of the different sensor types considered in the paper for single wave ocean environments. Numerical results supporting our findings were presented. To more realistically model waves from the real world, we plan to investigate the behavior of these networks in irregular ocean wave environments and present the findings in a later paper. Preliminary results from irregular environments indicate that several findings from this paper transfer over to cases with irregular waves. Other future work could extend the wave model to include nonlinearities or to remove other assumptions.

REFERENCES

[1] Li, G., Weiss, G., Mueller, M., Townley, S., and Belmont, M. R., 2012. "Wave energy converter control by wave prediction and dynamic programming". *Renewable Energy,* ***48***, pp. 392–403.

[2] Budal, K., Falnes, J., Hals, T., Iversen, L., and Onshus, T., 1981. "Model experiment with a phase controlled point absorber". In Proceedings of Second International Symposium on Wave and Tidal Energy, pp. 191–206.

[3] Budal, K., Falnes, J., Iversen, L. C., Lillebekken, P. M., Oltedal, G., Hals, T., Onshus, T., and Høy, A., 1982. "The norwegian wave-power buoy project".

[4] Morris, E., Zienkiewicz, H., Pourzanjani, M., Flower, J., and Belmont, M., 1992. "Techniques for sea-state prediction". In Proceedings of the Second International Conference on Manoeuvring and Control of Marine Craft, Southampton, pp. 547–571.

[5] Sand, S. E., 1979. *Three-dimensional deterministic structure of ocean waves*. Institute of Hydrodynamics and Hydraulic Engineering, Technical University of Denmark.

[6] Esteva, D., 1976. "Wave direction computations with three gage arrays". *Coastal Engineering Proceedings,* ***1***(15).

[7] Panicker, N., and Borgman, L. E., 1970. "Directional spectra from wave-gage arrays". *Coastal Engineering Proceedings,* ***1***(12).

[8] Benoit, M., Frigaard, P., and Schäffer, H. A., 1997. "Analyzing multidirectional wave spectra: a tentative classification of available methods". In Proceedings of the 1997 IAHR conference, San Francisco, The Johns Hopkins University Press, Baltimore, pp. 131–158.

[9] Falnes, J., 2002. *Ocean waves and oscillating systems: linear interactions including wave-energy extraction*. Cambridge University Press.

[10] Radhakrishna Rao, C., 1945. "Information and accuracy attainable in the estimation of statistical parameters". *Bulletin of the Calcutta Mathematical Society,* ***37***(3), pp. 81–91.

[11] Van Trees, H. L., 2004. *Detection, Estimation, and Modulation Theory, Optimum Array Processing*. Wiley-Interscience.

[12] Kay, S. M., 1993. "Fundamentals of statistical signal processing, volume i: Estimation theory (v. 1)".

[13] Marano, G. C., Monti, G., and Quaranta, G., 2011. "Comparison of different optimum criteria for sensor placement in lattice towers". *The Structural Design of Tall and Special Buildings,* ***20***(8), pp. 1048–1056.

[14] Helferty, J. P., and Mudgett, D. R., 1993. "Optimal observer trajectories for bearings only tracking by minimizing the trace of the cramer-rao lower bound". In Decision and Control, 1993., Proceedings of the 32nd IEEE Conference on, IEEE, pp. 936–939.